

www.acsnano.org

How a Virus Circumvents Energy Barriers to Form Symmetric Shells

Sanaz Panahandeh,* Siyu Li, Laurent Marichal, Rafael Leite Rubim, Guillaume Tresset, and Roya Zandi



Cite This: ACS Nano 2020, 14, 3170-3180



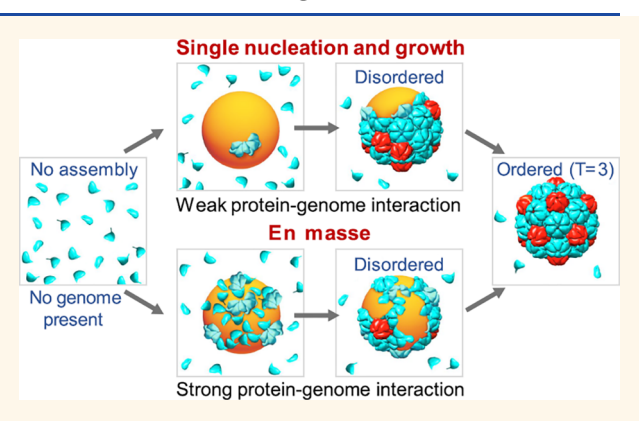
ACCESS I

Metrics & More

Article Recommendations

Supporting Information

ABSTRACT: Previous self-assembly experiments on a model icosahedral plant virus have shown that, under physiological conditions, capsid proteins initially bind to the genome through an en masse mechanism and form nucleoprotein complexes in a disordered state, which raises the question as to how virions are assembled into a highly ordered structure in the host cell. Using small-angle X-ray scattering, we find out that a disorder—order transition occurs under physiological conditions upon an increase in capsid protein concentrations. Our cryo-transmission electron microscopy reveals closed spherical shells containing *in vitro* transcribed viral RNA even at pH 7.5, in marked contrast with the previous observations. We use Monte Carlo simulations to explain this disorder—order transition and find that, as the shell grows, the structures of disordered intermediates in which the distribution of



pentamers does not belong to the icosahedral subgroups become energetically so unfavorable that the caps can easily dissociate and reassemble, overcoming the energy barriers for the formation of perfect icosahedral shells. In addition, we monitor the growth of capsids under the condition that the nucleation and growth is the dominant pathway and show that the key for the disorder—order transition in both en masse and nucleation and growth pathways lies in the strength of elastic energy compared to the other forces in the system including protein—protein interactions and the chemical potential of free subunits. Our findings explain, at least in part, why perfect virions with icosahedral order form under different conditions including physiological ones.

KEYWORDS: self-assembly, viral shells, elastic energy, kinetic pathways, nucleation

he process of formation of virus particles in which the protein subunits encapsidate genome (RNA or DNA) to form a stable, protective shell called the capsid is an essential step in the viral life cycle. The capsid proteins of many small single-stranded RNA viruses spontaneously package their wild-type (wt) and other negatively charged polyelectrolytes, a process basically driven by the electrostatic interaction between positively charged protein subunits and negatively charged cargo. Understanding the phenomena of formation of viral particles is of great interest due to their potential applications in nanomedicine and biomaterials. Capsids can be employed as nanocontainers, biosensors, nanoreactors, and drug or gene delivery vehicles to name just a few. September 2019.

Regardless of the virion size and assembly procedures, most spherical viruses adopt structures with icosahedral symmetry. The total number of proteins in an icosahedral capsid is equal to 60T, where T is the triangulation number assuming only certain integers (T = 1, 3, 4, 7,...). Some number of viruses follow a generalized principle of quasi-equivalence that

can be modeled via a combination of hexamers, pentamers, and trimers. We do not discuss this class of viruses as our focus is basically on T=3 structures in this paper. Independently of the number of proteins, there are always 12 pentagonal defects in a shell built from a triangular lattice sitting on the vertices of an icosahedron to preserve the symmetry of the capsid.

How exactly capsid proteins (CPs) assemble to assume a specific size and symmetry have been investigated for over half a century now. 14,15 As the self-assembly of virus particles involves a wide range of thermodynamics parameters, different time scales, and an extraordinary number of possible pathways, the kinetics of assembly has remained elusive, linked to

Received: October 22, 2019 Accepted: February 24, 2020 Published: March 2, 2020



Levinthal's paradox for protein folding. ^{16–18} The role of the genome on the assembly pathways and the structure of the capsid is even more intriguing. ^{3,19–22} The kinetics of virus growth in the presence of RNA is at least 3 orders of magnitude faster than that of empty capsid assembly, indicating that the mechanism of assembly of CPs around RNA might be quite different. Some questions then naturally arise: What is the role of RNA in the assembly process, and by what means then does RNA preserve assembly accuracy at fast assembly speed?

Two different mechanisms for the role of the genome have been proposed: (i) en masse assembly and (ii) nucleation and growth.^{23–25} Several years ago, McPherson suggested the "en masse" model in which the nucleic acid attracts CPs in solution to its surface through long-range electrostatic interactions. Note that the assembly interfaces in many CPs are principally short-ranged hydrophobic in character, whereas there is a strong electrostatic, nonspecific long-ranged interaction between RNA and CPs. To this end, the positively charged domains of CPs associate with the negatively charged RNA quite fast and form an amorphous complex. Hydrophobic interfaces then start to associate, which leads to the assembly of a perfect icosahedral shell. Based on the en masse mechanism, the assembly pathways correspond to situations in which intermediates are predominantly disordered.

More recently Chevreuil et al.²⁶ studied en masse assembly by carrying out time-resolved small-angle X-ray scattering (SAXS) experiments on cowpea chlorotic mottle virus (CCMV), a T = 3 single-stranded RNA plant virus. They found that, at neutral pH, a considerable number of CPs were rapidly (~28 ms) adsorbed to the genome, which more slowly (~48 s) self-organized into compact but amorphous nucleoprotein complexes (NPC) (see also ref 27). By lowering the pH, they observed a disorder-order transition as the protein-protein interaction became strong enough to close up the capsid and to overcome the high energy barrier ($\sim 20k_{\rm B}T$, where $k_{\rm B}$ is the Boltzmann constant and T is the temperature) separating NPCs from virions. It is important to note that a marked difference between in vitro and in vivo assemblies is that capsid proteins form ordered icosahedral structure at physiological pH (in vivo conditions), but until now, ordered structures are observed only at acidic pH in the in vitro selfassembly studies.²⁸⁻³⁰

Due to the electrostatic interaction between the genome and CPs, the en masse assembly is expected to be the dominant growth pathway. However a set of more recent experiments points to the nucleation-elongation mechanism. Garmann et al. have employed interferometric scattering microscopy to measure the assembly kinetics of single MS2 virus particles around MS2 RNA strands tethered to the surface of a coverslip. 30,31 Comparisons of individual assembly pathways indicated that most trajectories exhibit a sigmoidal time dependence, with plateau scattering intensity values similar to those acquired from complete particles. According to their experimental data, each trajectory is characterized by a lag time after which the assembly takes off, a signature of the nucleation-elongation mechanism. The measurements of Garmann et al. reveal that the lag time is not due to the diffusion of the CPs but is directly related to the nucleation and growth mechanism.31

Although the experiments of Chevreuil *et al.* clearly point to the en masse assembly mechanism, it is hard to explain how a transition from a disordered amorphous RNA—CP complex to

a highly ordered icosahedral capsid can take place where the location of pentamers is very precise and CP–CP interaction is around $-7k_{\rm B}T$. Further, the assembly through the nucleation and growth mechanism is not bound to follow an ordered pathway at all times; that is, a disorder—order transition might also occur as the shell grows. The molecular dynamic simulations of Elrad and Hagan have shed light on the assembly pathways of virus particles in the presence of the genome; ^{24,32} however, the simulations were designed such that only T=1 structures could form, whereas the kinetic pathways to the formation of slightly larger viruses such as T=3 and 4 are still elusive.

In this paper, we study the kinetic pathways of virus assembly using MC simulations and specifically elucidate the role of elastic energy in the disorder—order transition in T=3 viruses formed through either en masse or nucleation and growth mechanism. We, in particular, focus on the impact of protein concentration on the disorder—order transition. Through MC simulations and a set of experiments employing small-angle X-ray scattering and cryo-transmission electron microscopy, we explore the role of protein concentrations in the formation of T=3 structures of CCMV particles. Our findings shed light on the *in vivo* assembly of icosahedral structures and can explain to some extent why virion forms at neutral pH *in vivo*, whereas the acidic pH was so far required in the *in vitro* self-assembly studies of T=3 structures.

The paper is organized as follows. In the next section, we present the results of numerical simulations indicating the importance of elastic energy in the disorder—order transition. We also study the impact of protein concentration on the assembly pathway and compare it with our SAXS experiments. Next, we present our conclusion and summarize our findings. In the Methods section, we introduce the simulation approaches. Several details of calculations and experimental methods are relegated to the Supporting Information (SI).

RESULTS AND DISCUSSION

As noted in the introduction, two different mechanisms are proposed for the role of the genome in the assembly of viral shells: (1) nucleation and growth and (2) en masse assembly. We will decipher each in the following sections. Because of the extraordinary number of degrees of freedom involved in the assembly process, we focus only on understanding a number of recent experiments in which the genome has assumed different roles. We study the experiments of Garmann et al.31 to elucidate the process of nucleation and growth in the presence of the genome and then investigate the experiments of Chevreuil et al. to explore how the genome promotes the assembly through the en masse or a multinucleation mechanism.²⁶ In order to obtain a better understanding of the disorder-order transition, we perform a set of X-ray scattering experiments at neutral pH to study the role of protein concentration in the disorder-order transition and compare them with the results of our simulations. In what follows, we first present the results of our simulations for the single nucleation assembly and then show our experimental data and simulations corresponding to the multinucleation or en masse mechanism.

We emphasize that the main difference between the en masse and nucleation and growth mechanisms corresponds to their relevant time scales. In the en masse process, subunits bind to the genome in a short time frame, forming multiple patches or nuclei, and the structure keeps growing in a

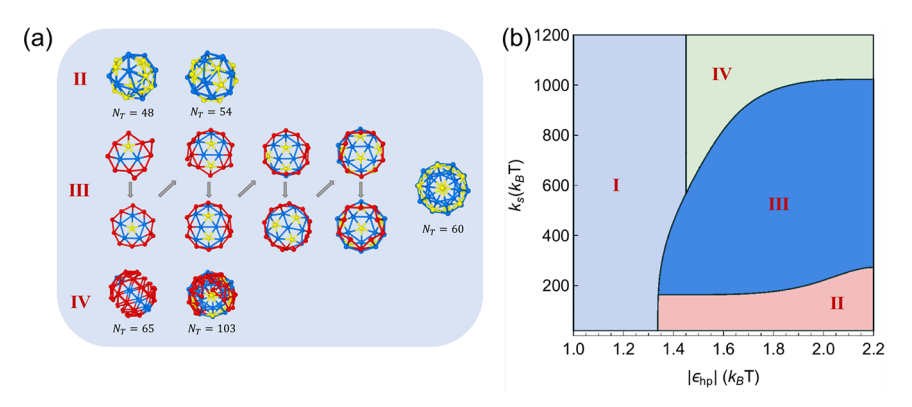


Figure 1. Phase diagram for the reversible growth model and snapshots of assembled structures as a function of stretching modulus, k_s , and monomer—monomer hydrophobic interaction, $\epsilon_{\rm hp}$. In region I, no shell forms due to lack of nucleation; in region II, capsids form irregular shapes with lower symmetries, and total trimer number, $N_{\rm T}$, is less than 60; in region III, only T=3 structures form. Snapshots of a representative pathway are illustrated in the panel (a) where pentamers first form at the boundary, and then the shell continues to grow around them. Images in panel (a) are made with OVITO.³⁹ The pathway is consistent and matches very well with the ground-state calculation corresponding to the locations of pentamers as a shell grows (see SI Figure S1). In region IV, the cost of stretching energy is so high that the structures cannot close but form messy shells. Other parameters of simulations are spontaneous radius $R_0=1.5$, bending rigidity $k_{\rm b}=200k_{\rm B}T$, and chemical potential $\mu=-14.6k_{\rm B}T$.

disordered manner. When enough subunits are adsorbed, they undergo cooperative rearrangements to assemble into an ordered capsid. By contrast, in the nucleation—elongation mechanism, the longer time scale corresponds to the formation of the first nucleus, and the shell grows by sequential binding of subunits to its edge. The growth phase is always shorter than the nucleation time. The assembly starts at one point and continues until an ordered shell is formed. Both en masse and nucleation—elongation pathways can involve a disorder—order transition.

Nucleation and Growth. We first investigate the assembly of empty capsids where the nucleation and growth is the dominant mechanism and then present our results on the single nucleation mechanism in the presence of the genome.

Empty Capsids. Based on eqs 7-9 in the Methods section, the total energy of an empty capsid can be written as

$$E_{\text{tot}} = E_{\text{el}} + E_{\text{hp}} - N_{\text{T}}\mu = (\epsilon_{\text{el}} + \epsilon - \mu)N_{\text{T}}$$
(1)

where $N_{\rm T}$ is the total number of trimers, $E_{\rm el}=E_{\rm s}+E_{\rm b}$ is the total elastic energy of the capsid, $E_{\rm hp}$ is the protein—protein interaction (basically hydrophobic), and μ is connected to the chemical potential of free proteins in solution. For a dilute system, $\mu=k_{\rm B}T\log\frac{\rho}{\rho_{\rm o}}$, with ρ being the density of free proteins in solution and $\rho_{\rm o}$ the reference density. The average elastic energy and attractive protein—protein interaction per subunit are denoted by $\epsilon_{\rm el}$ and $\epsilon_{\rm o}$, respectively.

Figure 1a,III illustrates the snapshots of simulations for the growth of an empty shell through the reversible pathway described in the Methods section. As the cap grows, at some point, the formation of pentamers becomes energetically unavoidable because of the spherical geometry of the shell. The first pentamer always forms in the vicinity of the cap edge, and then the shell grows around the pentamer such that, at the end, the pentamer is in the middle of the cap. The following pentamers appear as illustrated in the figure, and the shell grows around them. We note that the hydrophobic interaction always prefers that each subunit has the maximum number of neighbors, six. However, because of the shell curvature, this is not always possible. The stretching energy defines the position of pentamers and thus the symmetry of the shell.

Quite interestingly, the position of pentamers follows very well the prediction of continuum elasticity theory where the ground state energy of a spherical cap was calculated to obtain the optimal position of disclinations^{33,34} (see Figure S1). This confirms that the system is completely reversible, equilibrated, and is able to find the minimum energy structures along the pathway.

The fact that most spherical viruses adopt structures with icosahedral symmetry reveals the important role of elasticity in the energetics of viral shells. 34-36 Nevertheless, it has remained a mystery how an error-free shell formed out of 90 dimers or 60 trimers grows with perfect icosahedral symmetry under many different in vitro assembly conditions. One expects that when a considerable part of a shell is formed, the pentamers formed well inside the cap far from the edge will become more or less frozen at their locations. Thus, if a pentamer is formed in a "wrong" position, the icosahedral symmetry should permanently be broken. However, the reversible simulations show that, as a shell grows, the elastic energy can become strong enough to easily break the bonds for a wide range of hydrophobic interactions and repair the positions of pentamers formed in the locations not consistent with icosahedral subgroup symmetries.

If the elastic energy is too small or too large compared to the attractive interaction between subunits, the symmetry of the shell will also be broken. To explore the interplay of elasticity and the hydrophobic interaction between subunits in the final structure of shells, we construct a phase diagram for the spring modulus $k_{\rm s}$ ranging from $20k_{\rm B}T$ to $1200k_{\rm B}T$ and $|\epsilon_{\rm hp}| \in [1k_{\rm B}T, 2.2k_{\rm B}T]$, as illustrated in Figure 1b. The value of bending rigidity was chosen based on the experimental values obtained previously. Note that as long as the ratio of the stretching to bending modulus is larger than 1, the final assembly products do not depend on the bending modulus, which we have kept equal to $k_{\rm b} = 200k_{\rm B}T$ for all of the simulations. 37,38

In region I of the phase diagram in Figure 1, the hydrophobic interaction is so weak that no capsid could nucleate. In region II, the elastic energy is weak compared to the hydrophobic interaction, and the shell easily gets kinetically trapped and irregular structures form with the total number of subunits less than 60 (a T = 3 structure) (Figure 1a). One can

see that for a large region of the phase diagram (region III), the competition between elastic and hydrophobic energies is such that the final product is always a T=3 structure. As the elastic energy becomes stronger in region IV, even for very strong hydrophobic interactions, the shell is not able to close but assumes a structure with cylindrical symmetry and grows in a "branchy" way, forming a messy structure (Figure 1a). Whereas T=3 constitutes the minimum energy structure for the entire phase diagram, messy structures with no symmetry can readily form in different regions, as shown in Figure 1. It is not always possible to obtain T=3 structures without using different MC techniques to avoid local traps. We calculate the energy barrier to the formation of T=3 structures in the next section to explain why in some regions the shells can easily get trapped in a local minimum energy structure.

Figure 2 shows the snapshots of simulations of a cap in which two pentamers are formed next to each other at the

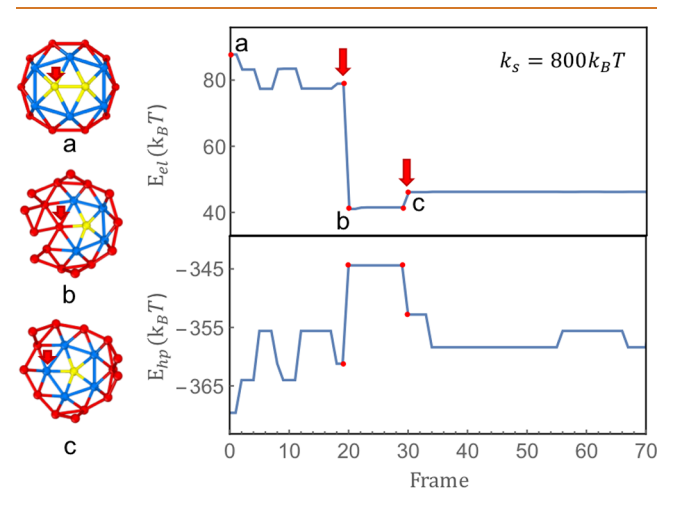


Figure 2. Snapshots of simulations for a partially formed capsid with 24 subunits. The right column shows the elastic and hydrophobic energies *versus* frame (number of MC moves) or time. (a) Two pentamers are formed in the vicinity of each other. (b) Around 20 MC steps due to high elastic energy (marked with a red arrow), a bond breaks to decrease the elastic energy while increasing the hydrophobic energy (point b in the energy plots). (c) Hexamer forms and slightly increases the elastic energy while decreasing the hydrophic energy. The protein subunits stretching rigidity is $k_{\rm s}=800k_{\rm B}T$ and bending rigidity $k_{\rm b}=200k_{\rm B}T$. Other parameters used are hydrophobic interaction $\epsilon_{\rm hp}=-1.4k_{\rm B}T$ and chemical potential $\mu=-14.6k_{\rm B}T$.

beginning of the assembly. The reversible growth allows the bonds to break and a pentamer to change to a hexamer as the assembled shell grows to have about 25 trimers. Note that the dynamics of the system specifically depends on the stretching modulus of subunits, $k_{\rm s}$. Lower stretching rigidity slows down the pentamer—hexamer transition, emphasizing the role of elasticity in the kinetic pathway of the assembly. Figure S2 shows that as $k_{\rm s}$ decreases from $800k_{\rm B}T$ to $200k_{\rm B}T$, it takes much longer for the system to repair the position of the pentamer.

Figure 2 clearly illustrates that the elastic energy of the shell decreases (indicated with an arrow) when the bonds of a "wrong" pentamer are broken. During this time, the hydrophobic energy increases, which is the penalty for breaking the bonds, resulting into an energy barrier to the formation of icosahedral shells. However, in this case, the elastic energy of

the shell is strong enough to overcome the local energy barriers and assume the symmetric structure. The total energy of the system is plotted in Figure S3. It is important to emphasize that the elastic energy diverges if a shell grows without pentamers.

At the end of this section, we emphasize that even though during the simulations one subunit was added at a time, our conclusion remains the same if several subunits join the growing shell simultaneously. The strength of elastic energy as the shell assembles makes the process reversible and the results robust, independent of the number of subunits joining the growing shell.

Classical Nucleation and Energy Barrier. To understand why closed structures without any particular symmetry appear in the phase diagram of Figure 1, where T=3 structure has the lowest energy, we calculate the energy barriers for the formation of T=3 in different regions of the diagram.

For a complete shell, the total hydrophobic interaction is $E_{\rm hp} = 15(Q-4)\epsilon_{\rm hp}$, where Q is the total number of subunits and $\epsilon_{\rm hp}$ is the monomer–monomer interaction as described in the Methods section. For a growing shell or a cap, the hydrophobic interaction in eq 9 becomes

$$E_{\rm hp} = \epsilon N_{\rm T} + \epsilon_{\rm l} \tag{2}$$

where $\epsilon_{\rm l}$ is the line tension. The average hydrophobic interaction per subunit is $\epsilon=15\epsilon_{\rm hp}\frac{Q-4}{Q}$ and converges to $15\epsilon_{\rm hp}$ as $Q\to +\infty$ (see Hydrophobic Interaction section in the SI). Combining eq 1 and eq 2, we obtain the free energy of the growing capsid as

$$\frac{E_{\text{tot}}}{|\epsilon|} = AN_{\text{T}} + a\sqrt{N_{\text{T}}(Q - N_{\text{T}})}$$
(3)

where $a=\frac{\sqrt{\alpha Q}}{Q-4}$ is a geometric factor, $\alpha=\frac{9\sqrt{3}\pi}{25}$ and $A=\frac{\epsilon_{\rm el}+\epsilon-\mu}{|\epsilon|}$ measures the difference between the chemical potentials of free subunits in solution and in full capsids (see the SI for more details). To make it dimensionless, we have divided it by the hydrophobic energy per subunit ϵ . For a T=3 structure

$$A = \frac{\epsilon_{\rm el} + 14\epsilon_{\rm hpp} - \mu}{|14\epsilon_{\rm hpp}|} \tag{4}$$

The height of energy barrier and the nucleation size can then be calculated through the maximum of the free energy as follows:

$$N_{\rm T}^* = \frac{1}{2} Q \left(1 + \frac{A}{\sqrt{A^2 + a^2}} \right)$$

$$E_{\rm tot}^* = \frac{1}{2} |\epsilon| Q \left(A + \sqrt{A^2 + a^2} \right)$$
(5)

Figure 3 shows the total free energy (eq 3) *versus* the number of subunits for $A \in (-0.5, 0.5)$ (eq 4) at three different values of the monomer—monomer hydrophobic interaction, $\epsilon_{\rm hp} = -1.0, -1.4$, and $-1.8k_{\rm B}T$. The figure reveals the impact of different thermodynamic parameters on the height of energy barriers. As illustrated in the figure, for a fixed $\mu = -14.6k_{\rm B}T$ and a given hydrophobic interaction $\epsilon_{\rm hp}$, the energy barrier increases when the elastic energy per subunit $\epsilon_{\rm el}$ increases (see eq 4).

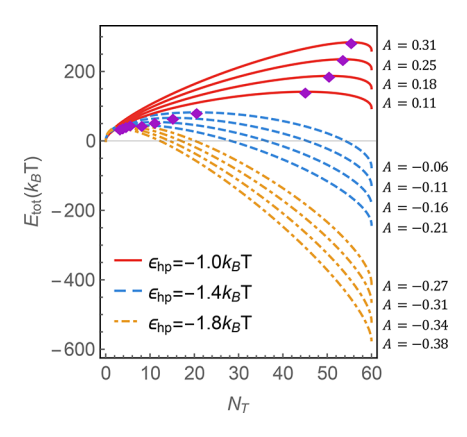


Figure 3. Total energy $E_{\rm tot}$ as a function of subunits. The energy barriers are indicated with diamonds. The value of coefficient A (eq 4) is indicated next to each curve. The stretching moduli used are $k_{\rm s}=800,\,600,\,400,\,$ and $200k_{\rm B}T$ (from top to bottom for each color). The chemical potential is $\mu=-14.6k_{\rm B}T,\,$ and the hydrophobic interaction is $\epsilon_{\rm hp}=-1.0k_{\rm B}T$ (solid), $-1.4k_{\rm B}T$ (dashed), and $-1.8k_{\rm B}T$ (dotted dashed).

The results shown in Figure 3 are consistent with the phase diagram presented in Figure 1 in that for $\mu=-14.6k_{\rm B}T$ if factor A is large because of the strong elastic energy and the small hydrophobic $\epsilon_{\rm hp}=-1k_{\rm B}T$, then the energy barrier is too high for the formation of capsids and no structure nucleates. Note that if the energy of the final product is positive, the symmetric shells are thermodynamically unstable and no capsids form. In fact, for $\epsilon_{\rm hp}=-1.0k_{\rm B}T$ regardless of stretching modulus, no capsid nucleates unless the chemical potential is at least $\mu=-10k_{\rm B}T$. On the other hand, when the hydrophobic interaction is too strong compared to the elastic energy, A is small and the nucleation size is less than five subunits, resulting in the formation of kinetically trapped smaller structures than T=3, corresponding to region II in the phase diagram.

In the next section, we present the growth of capsids in the presence of the genome through a nucleation and growth mechanism

Assembly in the Presence of the Genome. The self-assembly experiments of Garmann *et al.* indicate the assembly proceeds through the nucleation and growth mechanism with genome present.³¹ The process of nucleation and growth on the surface of a gold nanoparticle or condensed genome is very similar to that of an empty capsid. In the former case, we start the simulations assuming that one trimer is sitting on the core interacting attractively with it.

Mimicking the experiments of Garmann *et al.*, we assume that the concentration of proteins is such that the process is not diffusion limited; that is, there are enough proteins in the vicinity of genomes to form capsids. More specifically, we consider that the subunits diffuse from the solution to the core, but the duration of attachment of a single subunit to the core is smaller than the nucleation time. Thus, the delay in the assembly is just because of nucleation. To this end, we only focus on the assembly of proteins on the core and do not study the diffusion of proteins to the core. The total energy of the complexes of core and proteins can be written as

$$E_{\text{tot}} = E_{\text{lj}} + E_{\text{el}} + E_{\text{hp}} - N_{\text{T}}\mu = (-\epsilon_{\text{lj}} + \epsilon_{\text{el}} + \epsilon - \mu)N_{\text{T}}$$
(6)

where ϵ_{lj} is the depth of the Lennard-Jones (LJ) potential representing the core—protein interaction on the core surface. For simplicity, we always set $R_{core} = R_0$.

The results of simulations in the presence of the core are presented in Figure 4. For these sets of simulations, we have

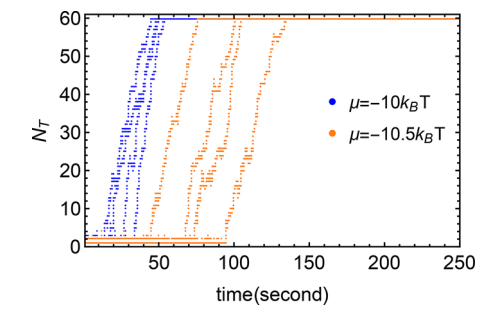


Figure 4. Several pathways for the formation of T=3 structures. The plot shows the number of subunits in the assembled caps as a function of time (seconds) for two different chemical potentials $\mu=-10~k_BT$ (blue) and $\mu=-10.5k_BT$ (orange). For each color, four different runs are shown, revealing fluctuations in the pathways of formation of T=3 icosahedral structures. The other parameters in simulations are $k_s=600k_BT$, $k_b=200k_BT$, $\epsilon_{\rm hp}=-1k_BT$, and the genome—protein interaction $\epsilon_{\rm lj}=1k_BT$. For these parameters, the assembly only proceeds through the nucleation and growth mechanism.

used the experiments of Garmann et al. to calibrate our MC steps to seconds.³¹ During the simulations, we observe that after about four or five subunits are assembled, the growth becomes very fast. As shown in the figure, it takes about 70 s on average for the $\mu = -10.5k_BT$ (orange lines) capsid to nucleate, which is followed by a rapid growth phase of 33 s. As the protein concentration goes higher ($\mu = -10k_BT$, blue lines), the nucleation time becomes shorter, about 24 s, and the rapid growth phase becomes about 25 s during which the capsid assembles to almost its final size. Note that, in these cases, in the absence of genome, no capsids could form. Changing μ from $-10.5k_BT$ to $-10k_BT$, we increase the protein concentration by 64% and observe that the nucleation time decreases about 65%. This is consistent at least qualitatively with the results of Garmann et al., 31 which according to their experiments, as the protein concentration changes from 1.5 to 2 μ M, the nucleation time decreases from about 160 to about 95 s. The results of our simulations also show that the growth time decreases with increasing protein concentration, but at a much slower rate than the nucleation time, as seen in the experiments.

If we increase the protein concentration even further to $\mu = -8k_{\rm B}T$, the chance of formation of another nucleus will be high and the process might become multinuclation or the en masse assembly, as will be explained in the next section. All of these simulations show that the interaction of capsid proteins with the genome facilitates the formation of capsids; that is, it lowers the energy barrier.

The above results reveal that, in the presence of the genome, even if the protein–protein interaction is not strong enough for the formation of empty capsids and the protein–genome interaction is weak such that the rate of detachment is larger than the rate of capsid nucleation, the combined effect of both interactions can give rise to the assembly of filled capsids. Note that if the presence of the genome decreases the energy barrier only by 1 or $2k_BT$, because of the associated Boltzmann factor,

the rate of formation of the capsid will increase by a factor of 3 or 4.

In the next section, we will study the en masse or multinucleation mechanism. First, we present our recent experiments and then the results of our simulations assuming that the protein–genome interaction is so strong that the proteins can get easily adsorbed to the genome and then nucleation occurs in different positions on the core.

En Masse Assembly. Experimental Evidence of a Disorder–Order Transition at Neutral pH. The kinetic studies of Chevreuil et al.²⁶ performed by mixing CCMV subunits (dimers of CPs) and the full (single-stranded RNA) genome at neutral pH showed that the assembly proceeded through the en masse rather than a single nucleation and growth process, and the final objects were amorphous nucleoprotein complexes (NPCs). Quite intriguingly, when the genome was replaced by a flexible, linear polyelectrolyte, namely, poly(stryrene sulfonic acid), 40,41 small but closed structures were formed, again via the en masse pathway. Why then cannot subunits form ordered structures in the presence of genomic RNA at neutral pH, which is yet physiologically relevant?

Figure 5 illustrates the effect of an increase in the concentration of subunits and genomic RNA on the structure

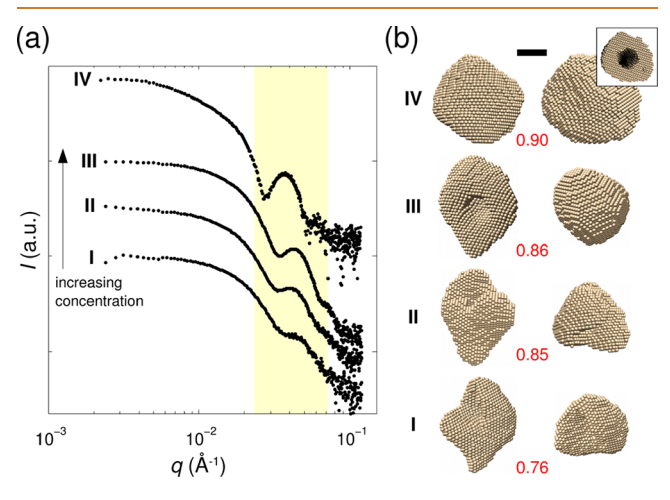


Figure 5. Equilibrium structure of NPCs at neutral pH and increasing concentrations in subunits and genomic RNA. (a) SAXS patterns obtained at a fixed subunit-to-RNA mass ratio of 6. Samples I, II, and III are made with the full CCMV genome at subunit concentrations of 0.5, 1.0, and 2.1 g·L⁻¹, respectively, whereas sample IV contains only *in vitro* transcribed CCMV RNA 2 for a subunit concentration of 2.1 g·L⁻¹. The yellow area highlights the growth of an interference peak in the curves due to an increasingly well-defined length scale in the scattering objects. The scattering curves are shifted for clarity. (b) *Ab initio* shape reconstructions carried out with the scattering curves in (a). The numbers in red are the sphericity indexes calculated for the corresponding structures. The inset is a cross-sectional view of the structure obtained for sample IV. Scale bar is 10 nm.

of NPCs at neutral pH. SAXS patterns of NPCs (Figure 5a) made with the full CCMV genome exhibit an increasingly pronounced interference peak in the medium q values as the concentrations are increased. The peak is even sharper when the full genome is replaced solely by *in vitro* transcribed RNA 2. The peak located around 0.04 Å⁻¹ corresponds to length scales around 15 nm and is associated with the spherical symmetry of virus-like objects. Lowering pH yields a similar

effect with the onset of two peaks, which are found at the same q values on the scattering curve of native virions at acidic pH (see SI Figure S6). The reconstructed shapes and their associated sphericity indexes (Figure 5b) suggest that the structures become more ordered and gradually acquire a spherical symmetry at high concentrations. Notice that the reconstructed shape of sample IV displays a hollow core (see inset of Figure 5b) like native virions. The reconstructed shapes must be considered with caution though, as they only provide ensemble-averaged, low-resolution structures and cannot reflect the actual variability between individual objects. Note that the analysis of the SAXS patterns by a polydisperse vesicle model (see SI Figure S5) also supports a higher degree of order at high concentrations.

In order to get a better insight into the morphology of the assembled objects, we perform cryo-transmission electron microscopy on a highly concentrated sample of NPCs made with *in vitro* transcribed RNA 2 because the SAXS patterns reveal objects with the highest sphericity index (Figure 5b). Quite consistently, the imaged objects (Figure 6) are mostly

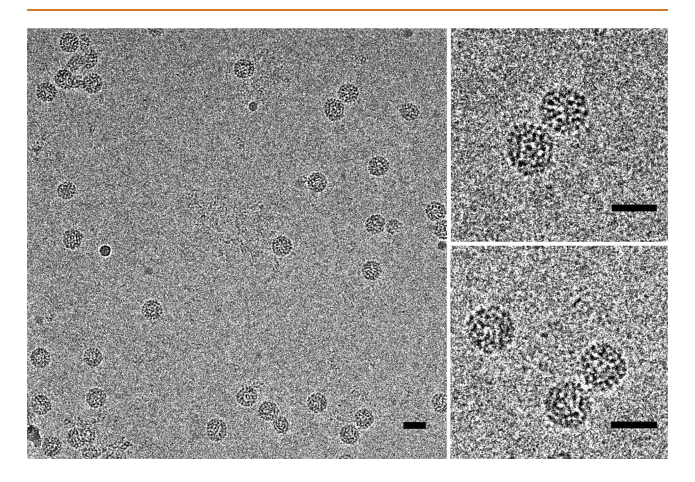


Figure 6. Cryo-transmission electron microscopy images of NPCs prepared at neutral pH. CCMV subunits are at a concentration of 3.9 g·L⁻¹, and *in vitro* transcribed CCMV RNA 2 is mixed at a subunit-to-RNA mass ratio of 6. Scale bars are 30 nm.

ordered and morphologically similar to native virions in these conditions, with a diameter around 30 nm. Some objects are still slightly disordered or aggregated. No empty spherical capsids are found, but we can see a few hollow nanotubes (see SI Figure S7) in agreement with the phase diagram of CCMV CPs at neutral pH.⁴³

In summary, our experimental studies show that a disorder—order transition occurs within NPCs upon an increase in subunits and genomic RNA concentrations, and that closed spherical shells packaging viral RNA can be assembled at neutral pH. These findings motivate us now to investigate theoretically the ability of the chemical potential to lower the energy barrier between NPCs and assembled virions.

Simulations. The snapshots of the growth of a capsid through en masse is illustrated in Figure 7. Right at the beginning of simulations, many subunits get adsorbed to the core and a messy structure forms (Figure 7a), similar to the NPCs observed in previous experiments ^{26,27} at pH 7.5 and the recent ones presented in the previous section. Special care is taken so that there is no overlap between subunits. We note that as for the simulations in which the nucleation and growth

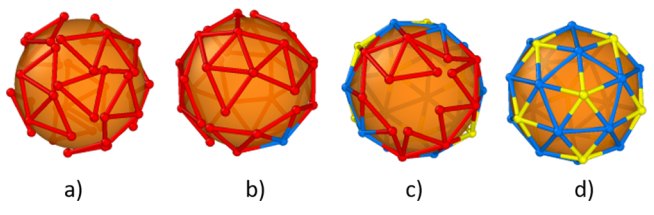


Figure 7. Snapshots of simulations in Figure 8. The chemical potential is $\mu = -14k_BT$, $k_s = 600k_BT$, $k_b = 200k_BT$, and $\epsilon_{li} =$ $11.2k_BT$. (a) View of an amorphous nucleoprotein complex after less than a second for $\epsilon_{hp} = -0.7k_BT$. There are around 20 subunits on the surface of the core. (b) View of a disordered structure. After 96 s, there are 40 trimers on the genome and multiple nuclei have formed. Later when the capsid has 45 trimers, we increase the hydrophobic strenght by changing $\epsilon_{\rm hp}$ from $-0.7k_{\rm B}T$ to $-1k_{\rm B}T$. This is consistent with the experiments when the pH is lowered from 7.5 to 5.2. (c) View of a partially formed capsid with 54 trimers after 5000 s. Subunits are relaxed to their lowest minimum energy positions. (d) Structure of a closed T = 3 capsid with 60 trimers. It takes around 14000 s for the capsid to complete. Red corresponds to vertices on the edge. Blue and yellow show the position of hexamers and pentamers, respectively. The images are made with OVITO.39

is the dominant mechanism, we do not study the diffusion of proteins into the genome in the case of en masse (or multinucleations) assembly either. More specifically, we consider that the assembly is reaction-limited, and thus the important time scale in the problem involves the addition of subunits to each other in order to form larger patches. Due to strong protein-genome interaction, we start simulations with about 10-15 subunits attached to the genome and consider that the growth proceeds basically through joining of the new subunits to other subunits already attached to the genome. Figure 7b shows a snapshot of the simulations when the interaction is weak ($\epsilon_{hp} = -0.7k_BT$), and the number of trimers is 40 with multiple nuclei already formed. We continue adding the subunits randomly to the edge of one of the existing subunits and accept the move as explained in the Methods section. The structure is still disordered.

The previous self-assembly experiments 26,27 showed that, when the pH is decreased, the attractive interaction between the protein subunits becomes stronger. Following the experimental steps, we also decrease $\epsilon_{\rm hp}$ from $-0.7k_{\rm B}T$ to $-1k_{\rm B}T$ when there are 45 trimers on the genome. At around 5000 s, 54 trimers are relaxed to their minimum energy positions in Figure 7c. The shell will form a T=3 structure around 14000 s (Figure 7d). The kinetics of assembly through the en masse pathway is illustrated in Figure 8 in the form of the number of subunits *versus* time. The behavior of the growth curves obtained in the en masse assembly is very similar to those of Chevreuil *et al.* in that, upon decreasing pH, a disordered to ordered transition occurs. We have employed the results of Figure 3a in ref 26 to calibrate the MC steps with time.

In addition to the pH change, the experiments presented in the previous section reveal the important role of protein concentrations in the disordered to ordered transition. To explore the impact of protein concentration and protein—protein interaction and to explain the experiments presented in Figure 5, we build a phase diagram for the formation of closed shells as a function of chemical potential and hydrophobic (attractive) interaction (see Figure 9).

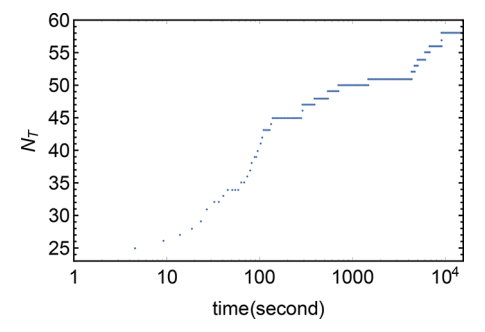


Figure 8. Number of subunits assembled around the genome *versus* time (seconds) for en masse (multinucleation) assembly at $\mu=-14k_{\rm B}T$, $k_{\rm s}=600k_{\rm B}T$, $k_{\rm b}=200k_{\rm B}T$, and $\epsilon_{\rm ij}=11.2k_{\rm B}T$. The number of subunits increases from 23 to around 45 trimers in the first 130 s, where the hydrophobic strength is weak ($\epsilon_{\rm hp}=-0.7k_{\rm B}T$). At $N_{\rm T}=45$, decreasing $\epsilon_{\rm hp}$ to $-1k_{\rm B}T$, the partially formed disordered capsid starts relaxing to the final structure with T=3 symmetry. The process of relaxation and reorganization to an ordered capsid takes around 14000 s.

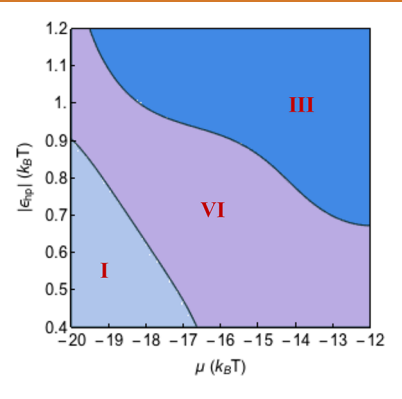


Figure 9. Phase diagram of structures obtained from en masse simulations for different values of chemical potentials and the strength of hydrophobic interactions. The strong genome—protein attractive interaction ($\epsilon_{\rm lj}=11.2k_{\rm B}T$) makes the assembly proceed through the en masse pathway. The blue corresponds to the region in which T=3 capsids form, but the purple one represents the phase where amorphous structures assemble. No capsid nucleates in the light blue region. As we move from left to right, the concentration of free subunits increases and we observe the disordered to ordered transition. The other parameters in the simulations are $k_{\rm s}=600k_{\rm B}T$, $k_{\rm b}=200k_{\rm B}T$, and the spontaneous radius $R_0=1.5$.

Figure 9 shows that for fixed $k_{\rm s}=600k_{\rm B}T$ and $k_{\rm b}=200k_{\rm B}T$, at high protein concentrations and strong protein—protein attractive interaction, only T=3 capsids form (region III). Note that if we increase both protein concentration and the strength of protein interaction significantly, the structures will be stuck in a local minimum energy and aberrant particles form (not shown in the phase diagram). In contrast at low hydrophobic interactions and low protein concentration, no structures nucleate (region I). We note that in the presence of packaging signals with high affinity for CP, the capsid forms even at very low protein concentration as the packaging signal increases the effective attractive interaction between the genome and proteins.

In the purple region (VI) of the diagram in Figure 9, only messy/amorphous structures form as observed in the experiments at pH 7.5. In this regime, the protein—protein interaction is not strong enough to form an ordered structure.

Nevertheless, the figure shows that for a fixed hydrophobic interaction, upon increasing protein concentrations, a disorder-order transition can occur; see for example the region around $\mu = -14k_{\rm B}T$ and $\epsilon_{\rm hp} = -0.8k_{\rm B}T$. As illustrated in the figure, if for $\epsilon_{\rm hp} = -0.8k_{\rm B}T$, the chemical potential increases from $-15k_{\rm B}T$ to $-13k_{\rm B}T$, one can observe the formation of T = 3 structures, consistent with the experimental results shown in Figure 5. It is worth mentioning that the transition from a disordered nucleoprotein complex to an icosahedral virion was reported several times by lowering the pH²⁶⁻²⁹ (see Figure S6), which is equivalent to increasing ϵ_{hp} for a fixed μ in Figure 11. The experiments in this paper correspond to the evidence of a disorder—order transition at a fixed $\epsilon_{\rm hp}$ —through fixed pH and ionic strength—by decreasing μ via the increase of subunit concentration. Consistent with the phase diagram depicted in Figure 9, SAXS measurements show that, upon an increase of subunit concentration (the subunit-to-RNA mass ratio is set to 6 in all cases), the nucleoprotein complexes become gradually ordered and cryo-TEM reveals the presence of a number of well-assembled virions at high concentration.

Quite interestingly, when we change the size of the core to be commensurate with a capsid, whose diameter is 23 nm consistently with the assembly experiments in the presence of PSS, we obtain a structure with the symmetry of a tennis ball (see SI Figure S8), which has been previously observed in self-assembly studies of clathrin shells.³⁵ The phase diagram for PSS is very similar to that for RNA, but the boundary lines between ordered—disordered configurations have moved (see Figure S9 in SI). We find that capsid proteins assemble to form closed shells at lower protein concentration that are needed for assembly with RNA. This behavior supports at least qualitatively the experimental results with PSS.²⁶

CONCLUSION

As during the assembly of viral particles, the intermediate states are transient and as such not easily accessible experimentally, the most fundamental questions about assembly pathways have remained unresolved. In this paper, we have focused on two different mechanisms observed in recent experiments: one supporting the en masse assembly and the other the nucleation and growth pathway.

Our results suggest at least in part that the elastic energy plays a crucial role in the assembly of error-free symmetric shells in both cases. We have found that, as a shell grows, if the pentamers form in the positions that break icosahedral order, through a reversible pathway, the pentamers can move to preserve the symmetry and form a T = 3 shell. This is counterintuitive as many bonds need to break for a pentamer formed far from the edge, well inside the capsid, to move. However, our results show that the elastic energy becomes so strong that as many bonds as necessary can be broken to move the pentamer (see Figure 2). Obviously, the relative strength of hydrophobic interaction and elastic energy is very important in this process (see Figures 1 and 3). Figure 10 shows a messy shell that was initially assembled fast in the presence of the high protein concentration. These sorts of shells can form either nucleation and growth or through the en masse pathway. Upon decreasing the protein concentration, we find that the shell relaxes to a T = 3 structure through a reversible pathway. The elastic energy indeed plays a crucial role in preserving the symmetry in transferring disordered to ordered structures.

The important role of protein concentration in the assembly pathway is summarized in Figure 11 for two different values of

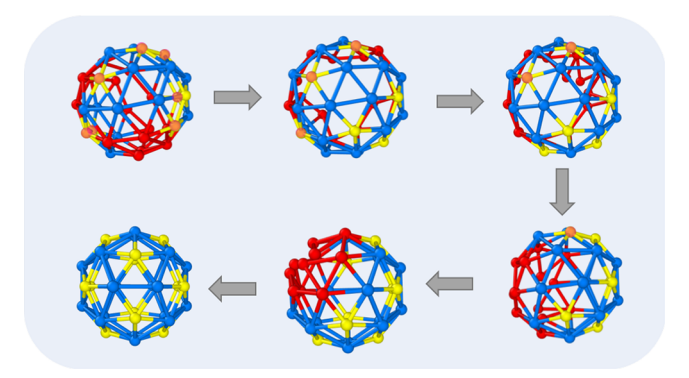


Figure 10. Relaxation of a messy shell to an icosahedral structure. At the beginning, the shell has 57 trimers with 7 pentamers formed in "wrong" positions (marked with orange). The shell relaxes to a T=3 capsid upon a change in pH or protein concentration. The blue, yellow, and red correspond to hexamers, pentamers, and the edge, respectively. The parameters used are stretching rigidity $k_{\rm s}=200k_{\rm B}T$, bending rigidity $k_{\rm b}=200k_{\rm B}T$, hydrophobic interaction $\epsilon_{\rm hp}=1.0k_{\rm B}T$, and chemical potential $\mu=-14k_{\rm B}T$. The images are made with OVITO. ³⁹

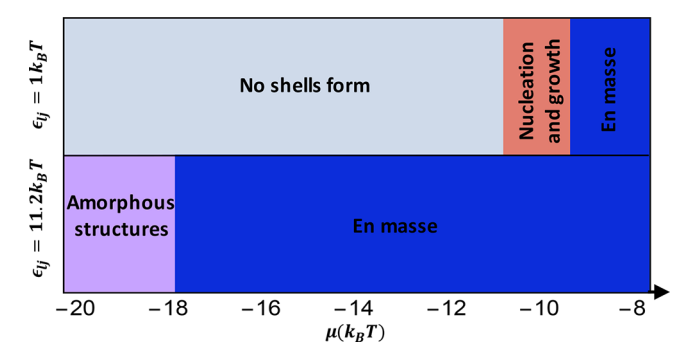


Figure 11. Capsids form with different mechanisms based on the strength of the protein–genome interaction. At a weak LJ interaction ($\epsilon_{\parallel}=1.0k_{\rm B}T$), for the chemical potentials between $-11k_{\rm B}T$ and $-9k_{\rm B}T$, capsids form through the nucleation and growth mechanism. For higher chemical potentials, the en masse assembly becomes the dominant pathway for the formation of T=3 structures. However, at strong LJ interaction ($\epsilon_{\parallel}=11.2k_{\rm B}T$), we obtain amorphous structures for low chemical potentials, but T=3 structures form through the en masse pathway for higher chemical potentials. Other parameters used in the simulations are $k_s=600k_{\rm B}T$, $k_b=200k_{\rm B}T$, and $\epsilon_{\rm hp}=-1k_{\rm B}T$.

genome—protein interaction, $\epsilon_{\rm lj}$. If the genome—protein interaction is weak, $\epsilon_{\rm lj}=1k_{\rm B}T$, for the low protein concentration, no shell nucleates. As the protein concentration increases, the shell grows through the nucleation and growth pathway. At higher concentrations, we observe that subunits get adsorbed onto the spherical core and the shell grows through the en masse assembly into a T=3 structure. In contrast for large $\epsilon_{\rm lj}=11.2k_{\rm B}T$ at low protein concentrations, amorphous structures form. Upon increasing protein concentration, ordered structures are obtained through the en masse assembly.

These results are consistent with our SAXS measurements at neutral pH, which clearly show an increasing degree of order upon the increase of concentration. Although even our best curves are not as regular as those obtained with native virions, in marked contrast with the previous experiments, we find that some structures look spherical and fully assembled at neutral pH. We note that the concentration may not be high enough

or other factors such as crowding effect or divalent cations may be important in the formation of icosahedral capsids, as well. Nevertheless, our experimental and numerical results clearly demonstrate that the chemical potential can significantly lower the energy barrier between amorphous complexes and virions, and it must have definitively a role in the *in vivo* assembly, as well.

METHODS

Simulations. To study the growth of viral shells, we use a coarse-grained model in which we focus on the fact that viral capsids are formed basically from hexamers and pentamers. The simplest building blocks that have been extensively used to model viruses and other protein nanocages are trimers. ^{6,45,46} The model allows us to discretize the growing elastic shell with triangular subunits, each consisting of three monomers, one sitting at the corner of each triangle. ³⁵

The total energy of a growing shell is the sum of the attractive interaction between subunits $E_{\rm hp}$ and the stretching $E_{\rm s}$ and bending $E_{\rm b}$ energies as follows:

$$E_{s} = \sum_{l_{i}} \frac{1}{2} k_{s} (b_{l_{i}} - b_{0})^{2} \tag{7}$$

$$E_{b} = \sum_{\langle t_{i}, t_{j} \rangle} k_{b} [1 - \cos(\theta_{\langle t_{i}, t_{j} \rangle} - \theta_{0})]$$
(8)

$$E_{\rm hp} = \sum_{\nu_i} \epsilon_{\rm hp} [nt_{\nu_i} (nt_{\nu_i} - 1)] \tag{9}$$

where the stretching energy sums over all edges l_i with b_0 the equilibrium length set equal to 1. Thus, b_{l_i} is a dimensionless quantity and $k_{\rm s}$ as the stretching modulus has the unit of energy. The bending energy involves the dihedral angle $\theta_{\left\langle t_i,t_i\right\rangle}$ between two connected trimers indexed by t_i and t_j such that $\cos\theta_{\left\langle t_i,t_j\right\rangle}=\hat{n}_{t_i}\hat{n}_{t_j}$ with \hat{n}_{t_i} and \hat{n}_{t_j} being the unit normal vectors of the trimers. The bending rigidity is $k_{\rm b}$

and
$$\theta_0=2\arcsin\!\left(\!\frac{b_0}{\sqrt{12R_0^2-3b_0^2}}\!\right)$$
 is the preferred dihedral angle related

to the spontaneous radius of curvature R_0 .⁴⁷ The attractive energy due to the hydrophobic interaction sums over all vertices ν_{ν} with $\epsilon_{\rm hp}$ being the strength of the monomer–monomer interaction. The range of hydrophobic interaction is considered to be small so that each vertex only interacts with its nearest neighbor vertices. The number of connected trimers is denoted by nt_{ν_i} for any vertex ν_i . We note that the interaction between subunits is due to both the hydrophobic interactions and electrostatic repulsion between subunits.⁴⁸ As the resultant force is attractive for the viruses to assemble, for brevity, we call it the hydrophobic interaction in the rest of the paper.

We emphasize that the hydrophobic interaction is the reason why proteins aggregate and attract each other, and thus it is negative. However, the stretching energy is due to the deviation of subunits from their equilibrium shape, and as such, it is positive. We note that other parameters like the geometry of the building blocks or vibrational modes could also have an impact on the growth pathway, but our focus in this paper is mainly on the impact of elastic energy.

Using Monte Carlo (MC) simulations, we monitor the growth of a viral shell through reversible steps. ⁴⁶ We consider three different MC moves: (1) diffusion, (2) attachment or detachment, and (3) merging or disjointing.

During the diffusion process, the number of capsid subunits remains fixed, corresponding to a canonical system. At each MC step, either a trimer or a vertex is chosen randomly (see Figures 12 and 13). The move is accepted with the probability $p_{\rm m}=\min(1,e^{-\beta E})$ with $\beta=1/k_{\rm B}T$ and E is the change in the total energy of the system after relaxation. The diffusion of trimers in Figure 12 could be considered as a combination of detachment and growth for trimers, the result of which should be qualitatively the same as diffusion in the canonical ensemble. The diffusion stops based on the convergence of the energy

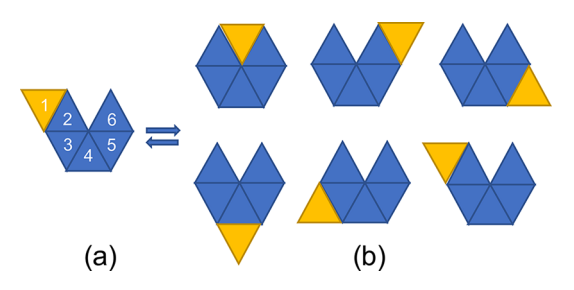


Figure 12. Schematic presentation of diffusion of a trimer around the shell edge. (a) Trimer 1 (yellow) is chosen randomly to diffuse around the edge. In this case, only trimers 1 and 6 are allowed to move during the diffusion mode. Trimers 2–5 are connected such that a few bonds need to be broken before they can diffuse. (b) Possible locations for trimer 1 to diffuse.

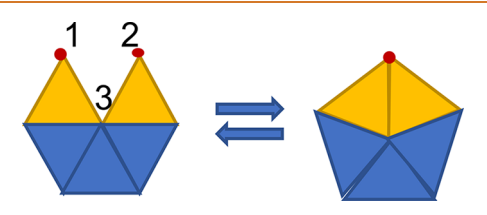


Figure 13. Schematic of vertex diffusion: vertices 1 and 2 merge to form a pentamer. The action is reversible in that both merging (left to right arrow) and disjointing (right to left arrow) are possible in the Monte Carlo moves.

of the system. The arrows in Figure 13 indicate the reversibility of each action.

After the diffusion step, a subunit will be added or removed with the probability p_g and p_d respectively. The probability of growth follows the detailed balance of the grand canonical ensemble with $p = \min\left(1, \frac{T_g}{T_g}e^{\beta\mu-\beta\Delta E}\right)$ and the probability of removal is

$$p_{\rm g}=\min\left(1,rac{T_{\rm g}}{T_{
m d}}e^{eta\mu-eta\Delta E}
ight)$$
 and the probability of removal is $p_{d}=\min\left(1,rac{T_{
m d}}{T_{
m g}}e^{-eta\mu-eta\Delta E}
ight)^{.49}$ The possible growth and detachment

sites are denoted by $T_{\rm g}$ and $T_{\rm d}$, respectively (see SI for more details). We note that by monitoring the assembly of proteins around the genome in most experiments, RNA condenses into its final size much faster than the other time scales involved in the process. 26,30,50 Thus, we replace the genome with a spherical core as the goal of this paper is basically on how the shell overcomes many energy barriers to form symmetric structures and not on the genome configurations. We note that if the experiments were performed in the diffusion-limited regime, we could not simply replace RNA with a spherical core.

Replacing the genome by a spherical core will decrease many degrees of freedom in the system, allowing us to focus carefully on the energetics involved in the assembly of viral shells. Thus, we consider a spherical core interacting through LJ with the capsid proteins

$$E_{lj} = \sum_{\nu_i} \epsilon_{lj} \left[\left(\frac{\sigma_{lj}}{r_{(\nu_i,g)}} \right)^{12} - 2 \left(\frac{\sigma_{lj}}{r_{(\nu_i,g)}} \right)^{6} \right], \text{ where } \epsilon_{lj} \text{ is the potential strength}$$

and $r_{\langle v_n g \rangle}$ is the distance between the core center and the triangle vertex v_i .

ASSOCIATED CONTENT

Supporting Information

The Supporting Information is available free of charge at https://pubs.acs.org/doi/10.1021/acsnano.9b08354.

Additional nine supporting figures, a supporting table, and more details regarding the elastic energy of a spherical cap as a function of θ_c ; two examples of disorder—order transitions with different spring constants; the plot of the total energy *versus* frame number;

plots of line tensions *versus* number of subunits; derivation of eqs 5 and 6 in the main text; SAXS patterns of NPCs fitted with a polydisperse vesicle model and table of fitting parameters for the SAXS patterns; form factors of NPCs and virions at acidic pH; cryo-transmission electron microscopy images of nanotubes; the structure and phase diagram for assembly of capsid proteins around the smaller core size (PDF)

AUTHOR INFORMATION

Corresponding Author

Sanaz Panahandeh — Department of Physics and Astronomy, University of California, Riverside, California 92521, United States; © orcid.org/0000-0001-9253-4891; Email: spana002@ucr.edu

Authors

Siyu Li — Department of Physics and Astronomy, University of California, Riverside, California 92521, United States Laurent Marichal — Université Paris-Saclay, CNRS, Laboratoire de Physique des Solides, 91405 Orsay, France

Rafael Leite Rubim – Université Paris-Saclay, CNRS, Laboratoire de Physique des Solides, 91405 Orsay, France

Guillaume Tresset — Université Paris-Saclay, CNRS, Laboratoire de Physique des Solides, 91405 Orsay, France; orcid.org/0000-0002-3755-4109

Roya Zandi – Department of Physics and Astronomy, University of California, Riverside, California 92521, United States

Complete contact information is available at: https://pubs.acs.org/10.1021/acsnano.9b08354

Notes

The authors declare no competing financial interest.

ACKNOWLEDGMENTS

This work was supported by the NSF through Awards DMR-1719550. The plasmid coding for the CCMV RNA 2 was kindly provided by Christian Beren from William Gelbart's group at the University of California Los Angeles. G.T. acknowledges financial support from the Agence Nationale de la Recherche (Contract ANR-16-CE30-0017-01). The electron microscopy imaging is supported by "Investissements d'Avenir" LabEx PALM (Contract ANR-10-LABX-0039-PALM), and we thank Jéril Degrouard for his technical assistance with the microscope. L.M., R.L.R., and G.T. also acknowledge the European Synchrotron Radiation Facility (ESRF) and the SOLEIL synchrotron for allocation of synchrotron beam time on ID02 and SWING beamlines.

REFERENCES

- (1) Flint, S.; Enquist, L.; Krug, R.; Racaniello, V.; Skalka, A. *Principles of Virology: Molecular Biology, Pathogenesis, and Control*; ASM Press: Washington D.C., 2000; pp 66–83.
- (2) Sun, J.; DuFort, C.; Daniel, M.-C.; Murali, A.; Chen, C.; Gopinath, K.; Stein, B.; De, M.; Rotello, V. M.; Holzenburg, A.; Kao, C. C.; Dragnea, B. Core-Controlled Polymorphism in Virus-Like Particles. *Proc. Natl. Acad. Sci. U. S. A.* **2007**, *104*, 1354–1359.
- (3) Siber, A.; Podgornik, R. Nonspecific Interactions in Spontaneous Assembly of Empty Versus Functional Single-Stranded RNA Viruses. *Phys. Rev. E* **2008**, *78*, 051915.
- (4) Erdemci-Tandogan, G.; Wagner, J.; Van Der Schoot, P.; Podgornik, R.; Zandi, R. RNA Topology Remolds Electrostatic Stabilization of Viruses. *Phys. Rev. E* **2014**, *89*, 032707.

- (5) Erdemci-Tandogan, G.; Wagner, J.; Van Der Schoot, P.; Podgornik, R.; Zandi, R. Effects of RNA Branching on the Electrostatic Stabilization of Viruses. *Phys. Rev. E: Stat. Phys., Plasmas, Fluids, Relat. Interdiscip. Top.* **2016**, *94*, 022408.
- (6) Vernizzi, G.; Sknepnek, R.; Olvera de la Cruz, M. Platonic and Archimedean Geometries in Multicomponent Elastic Membranes. *Proc. Natl. Acad. Sci. U. S. A.* **2011**, *108*, 4292–4296.
- (7) Zlotnick, A.; Aldrich, R.; Johnson, J. M.; Ceres, P.; Young, M. J. Mechanism of Capsid Assembly for an Icosahedral Plant Virus. *Virology* **2000**, *277*, 450.
- (8) Perlmutter, J. D.; Qiao, C.; Hagan, M. F. Viral Genome Structures Are Optimal for Capsid Assembly. *eLife* **2013**, *2*, e00632.
- (9) Mohajerani, F.; Hagan, M. F. The Role of the Encapsulated Cargo in Microcompartment Assembly. *PLoS Comput. Biol.* **2018**, *14*, e1006351.
- (10) Weiss, P. Armor-Plated Puzzle: Deciphering the Code of Viral Geometry. *Sci. News* **2005**, *168*, 152–154.
- (11) Johnson, J. E.; Speir, J. A. Quasi-Equivalent Viruses: A Paradigm for Protein Assemblies. *J. Mol. Biol.* **1997**, 269, 665–675.
- (12) Caspar, D. L.; Klug, A. Physical Principles in the Construction of Regular Viruses. *Cold Spring Harbor Symp. Quant. Biol.* **1962**, 27, 1–24
- (13) Twarock, R.; Luque, A. Structural Puzzles in Virology Solved with an Overarching Icosahedral Design Principle. *Nat. Commun.* **2019**, *10*, 4414.
- (14) Bancroft, J. B. The Self-Assembly of Spherical Plant Viruses. *Adv. Virus Res.* **1970**, *16*, 99.
- (15) Chen, T.; Zhang, Z.; Glotzer, S. C. A Precise Packing Sequence for Self-Assembled Convex Structures. *Proc. Natl. Acad. Sci. U. S. A.* **2007**, *104*, 717.
- (16) Asor, R.; Selzer, L.; Schlicksup, C. J.; Zhao, Z.; Zlotnick, A.; Raviv, U. Assembly Reactions of Hepatitis B Capsid Protein into Capsid Nanoparticles Follow a Narrow Path through a Complex Reaction Landscape. *ACS Nano* **2019**, *13*, 7610.
- (17) Levinthal, C. How to Fold Graciously. Mossbauer Spectroscopy in Biological Systems 1969, 67, 22-24.
- (18) Dykeman, E. C.; Stockley, P. G.; Twarock, R. Solving a Levinthal's Paradox for Virus Assembly Identifies a Unique Antiviral Strategy. *Proc. Natl. Acad. Sci. U. S. A.* **2014**, *111*, 5361–5366.
- (19) May, E. R. Recent Developments in Molecular Simulation Approaches to Study Spherical Virus Capsids. *Mol. Simul.* **2014**, *40*, 878–888.
- (20) Singaram, S. W.; Garmann, R. F.; Knobler, C. M.; Gelbart, W. M.; Ben-Shaul, A. Role of RNA Branchedness in the Competition for Viral Capsid Proteins. *J. Phys. Chem. B* **2015**, *119*, 13991.
- (21) Tubiana, L.; Bozic, A. L.; Micheletti, C.; Podgornik, R. Synonymous Mutations Reduce Genome Compactness in Icosahedral ssRNA Viruses. *Biophys. J.* **2015**, *108*, 194.
- (22) Erdemci-Tandogan, G.; Orland, H.; Zandi, R. RNA Base Pairing Determines the Conformations of RNA Inside Spherical Viruses. *Phys. Rev. Lett.* **2017**, *119*, 188102.
- (23) Larson, S. B.; McPherson, A. Satellite Tobacco Mosaic Virus RNA: Structure and Implications for Assembly. *Curr. Opin. Struct. Biol.* **2001**, *11*, 59.
- (24) Hagan, M. F. Modeling Viral Capsid Assembly. Adv. Chem. Phys. 2014, 155, 1.
- (25) Perlmutter, J. D.; Perkett, M. R.; Hagan, M. F. Pathways for Virus Assembly Around Nucleic Acids. *J. Mol. Biol.* **2014**, *426*, 3148–3165.
- (26) Chevreuil, M.; Law-Hine, D.; Chen, J.; Bressanelli, S.; Combet, S.; Constantin, D.; Degrouard, J.; Möller, J.; Zeghal, M.; Tresset, G. Nonequilibrium Self-Assembly Dynamics of Icosahedral Viral Capsids Packaging Genome or Polyelectrolyte. *Nat. Commun.* **2018**, *9*, 3071.
- (27) Garmann, R. F.; Comas-Garcia, M.; Knobler, C. M.; Gelbart, W. M. Physical Principles in the Self-Assembly of a Simple Spherical Virus. *Acc. Chem. Res.* **2016**, *49*, 48–55.
- (28) Garmann, R. F.; Comas-Garcia, M.; Gopal, A.; Knobler, C. M.; Gelbart, W. M. The Assembly Pathway of an Icosahedral Single-

- Stranded RNA Virus Depends on the Strength of Inter-Subunit Attractions. J. Mol. Biol. 2014, 426, 1050–1060.
- (29) Cadena-Nava, R. D.; Comas-Garcia, M.; Garmann, R. F.; Rao, A.; Knobler, C. M.; Gelbart, W. M. Self-Assembly of Viral Capsid Protein and RNA Molecules of Different Sizes: Requirement for a Specific High Protein/RNA Mass Ratio. *J. Virol.* **2012**, *86*, 3318—3326
- (30) Daniel, M. C.; Tsvetkova, I. B.; Quinkert, Z. T.; Murali, A.; De, M.; Rotello, V. M.; Kao, C. C.; Dragnea, B. Role of Surface Charge Density in Nanoparticle-Templated Assembly of Bromovirus Protein Cages. ACS Nano 2010, 4, 3853.
- (31) Garmann, R. F.; Goldfain, A. M.; Manoharan, V. N. Measurements of the Self-Assembly Kinetics of Individual Viral Capsids Around Their RNA Genome. *Proc. Natl. Acad. Sci. U. S. A.* **2019**, *116*, 22485–22490.
- (32) Elrad, O. M.; Hagan, M. F. Encapsulation of a Polymer by an Icosahedral Virus. *Phys. Biol.* **2010**, *7*, 045003.
- (33) Li, S.; Zandi, R.; Travesset, A.; Grason, G. M. Ground States of Crystalline Caps: Generalized Jellium on Curved Space. *Phys. Rev. Lett.* **2019**, *123*, 145501.
- (34) Li, S.; Roy, P.; Travesset, A.; Zandi, R. Why Large Icosahedral Viruses Need Scaffolding Proteins. *Proc. Natl. Acad. Sci. U. S. A.* **2018**, *115*, 10971–10976.
- (35) Wagner, J.; Zandi, R. The Robust Assembly of Small Symmetric Nanoshells. *Biophys. J.* **2015**, *109*, 956–965.
- (36) Panahandeh, S.; Li, S.; Zandi, R. The Equilibrium Structure of Self-Assembled Protein Nano-Cages. *Nanoscale* **2018**, *10*, 22802–22809.
- (37) Roos, W.; Bruinsma, R.; Wuite, G. Physical Virology. *Nat. Phys.* **2010**, *6*, 733.
- (38) Zeng, C.; Hernando-Pérez, M.; Dragnea, B.; Ma, X.; Van Der Schoot, P.; Zandi, R. Contact Mechanics of a Small Icosahedral Virus. *Phys. Rev. Lett.* **2017**, *119*, 038102.
- (39) Stukowski, A. Visualization and Analysis of Atomistic Simulation Data With OVITO-The Open Visualization Tool. *Modell. Simul. Mater. Sci. Eng.* **2010**, *18*, 015012.
- (40) Hu, Y.; Zandi, R.; Anavitarte, A.; Knobler, C. M.; Gelbart, W. M. Packaging of a Polymer by a Viral Capsid: The Interplay between Polymer Length and Capsid Size. *Biophys. J.* **2008**, *94*, 1428–1436.
- (41) Tresset, G.; Tatou, M.; Le Coeur, C.; Zeghal, M.; Bailleux, V.; Lecchi, A.; Brach, K.; Klekotko, M.; Porcar, L. Weighing Polyelectrolytes Packaged in Viruslike Particles. *Phys. Rev. Lett.* **2014**, *113*, 128305.
- (42) Fox, J. M.; Wang, G.; Speir, J. A.; Olson, N. H.; Johnson, J. E.; Baker, T. S.; Young, M. J. Comparison of the Native CCMV Virion with In Vitro Assembled CCMV Virions by Cryoelectron Microscopy and Image Reconstruction. *Virology* **1998**, 244, 212–218.
- (43) Lavelle, L.; Gingery, M.; Phillips, M.; Gelbart, W. M.; Knobler, C. M.; Cadena-Nava, R. D.; Vega-Acosta, J. R.; Pinedo-Torres, L. A.; Ruiz-Garcia, J. Phase Diagram of Self-Assembled Viral Capsid Protein Polymorphs. *J. Phys. Chem. B* **2009**, *113*, 3813–3819.
- (44) Stockley, P. G.; Twarock, R.; Bakker, S. E.; Barker, A. M.; Borodavka, A.; Dykeman, E.; Ford, R. J.; Pearson, A. R.; Phillips, S. E.; Ranson, N. A.; Tuma, R. Packaging Signals in Single-Stranded RNA Viruses: Nature's Alternative to a Purely Electrostatic Assembly Mechanism. J. Biol. Phys. 2013, 39, 277–287.
- (45) Siber, A.; Zandi, R.; Podgornik, R. Thermodynamics of Nanospheres Encapsulated in Virus Capsids. *Phys. Rev. E* **2010**, *81*, 051919.
- (46) Rotskoff, G. M.; Geissler, P. L. Robust Nonequilibrium Pathways to Microcompartment Assembly. *Proc. Natl. Acad. Sci. U. S. A.* **2018**, *115*, 6341–6346.
- (47) Hicks, S. D.; Henley, C. Irreversible Growth Model for Virus Capsid Assembly. *Phys. Rev. E* **2006**, *74*, 031912.
- (48) Kegel, W. K.; van der Schoot, P. Competing Hydrophobic Van Der Schoot, P. Competing Hydrophobic and Screened-Coulomb Interactions in Hepatitis B Virus Capsid Assembly. *Biophys. J.* **2004**, *86*, 3905–3913.

- (49) Frenkel, D.; Smit, B. Understanding Molecular Simulation: From Algorithms to Applications; Elsevier: San Diego, CA, 2001; Vol. 1.
- (50) Borodavka, A.; Tuma, R.; Stockley, P. G. Evidence That Viral RNAs Have Evolved for Efficient, Two-Stage Packaging. *Proc. Natl. Acad. Sci. U. S. A.* **2012**, *109*, 15769–15774.